THE JOURNAL OF PHYSICAL CHEMISTRY Letters

Letter

pubs.acs.org/JPCL

Realistic Surface Descriptions of Heterometallic Interfaces: The Case of TiWC Coated in Noble Metals

Christopher H. Hendon,*[,†] Sean T. Hunt,[†] Maria Milina,[†] Keith T. Butler,[‡] Aron Walsh,[¶,§] and Yuriy Román-Leshkov*[,†]

[†]Department of Chemical Engineering, Massachusetts Institute of Technology, Cambridge, Massachusetts 02139, United States

[‡]Department of Chemistry, University of Bath, Claverton Down, BA2 7AY Bath, United Kingdom

[¶]Department of Materials, Imperial College London, SW7 2AZ London, United Kingdom

[§]Department of Materials Science and Engineering, Yonsei University, Seoul, South Korea

Supporting Information

ABSTRACT: Noble metal-coated core−shell nanoparticles have been applied to a suite of catalytic applications, with the aim of decreasing the noble metal loading while ideally improving their performance. The chemistry and therefore activity at the surface of these materials are intimately related to the accurate description of the core−shell interface. Using density functional theory, we developed a procedure to obtain realistic surface topology descriptions at the heterometallic junction. This procedure was applied to a topical series of catalysts: $Ti_{0.1}W_{0.9}C$ coated in atomically thin monolayers of noble metals. Our quantum chemical calculations provide access to both relevant surface descriptions of these materials and also rationalize several experimental observations. Our general procedure paves the way for the rationalization and prediction of next-generation heterometallic catalysts.

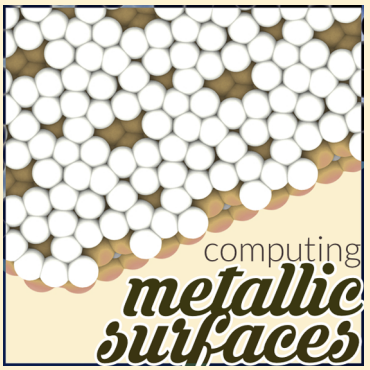

Core−shell nanoparticles, wherein an earth-abundant and inexpensive core material is coated with an atomically thin monolayer shell of noble metals (NMs), are an exciting and promising new design platform for catalysts with improved performance and reduced NM loadings compared to bulk NM nanoparticles.[1−4] Manipulation of the shell thickness, core size, and core−shell compositions could allow unparalleled control over catalytic activity and long-term durability. However, obtaining independent synthetic control over these parameters has proved challenging. The design of a suitable core material that affords strong shell−core interfacial bonding without negatively impacting the surface electronics of the shell would provide a major breakthrough in the field.[5,6] Additionally, the core material must have a high melting point to mitigate sintering, and the noble metal shell must remain insoluble in the core lattice to maintain high dispersion over the life of the catalyst. Recently, we developed a general procedure for synthesizing core−shell architectures of noble metals coated on transition-metal carbide (TMC) nanoparticles that satisfy these constraints.[7−10] In particular, titanium tungsten carbide (nominal stoichiometry, fcc-$Ti_{0.1}W_{0.9}C$) was found to be an excellent support because it favorably modulated the electronic properties of the shell to form electro- and thermocatalysts featuring higher activity. In addition, the insolubility of NMs in the TMC core resulted in highly stable materials that maintain the desired core−shell architecture.[9,11−15] Furthermore, we demonstrated that we could synthesize a variety of core and shell compositions, with highly controlled loadings of noble metals, gaining access to a broad array of core−shell catalysts with potentially tunable catalytic performance.

Because of the complexity of feasible descriptions of material surfaces, the nature of the NM−TMC interface is poorly understood. In particular, conventional models suffer from insufficient descriptions of the multitude of crystal facets and their surface interfaces with other metallic materials. Density functional theory (DFT) can be used to gain insights into both the characteristics of this interfacial bonding as well as the nature of stable and unstable core−shell interactions. In addition, computational chemistry can be harnessed as a powerful tool for directing the design of this new class of core−shell architectures through predictions of how transition-metal carbides can modulate the surface reactivity of noble metal monolayers.

The electronic properties of core−shell structures depend on both the identities of the components and the diameter and thickness of the core and shell, respectively. The alignment of the Fermi level (E_{Fermi}) to the vacuum level yields the work function (Φ).[16−18] The aligned E_{Fermi} allows a first approximation for the energetics of the interface,[19] and may be a factor in describing catalytic rates.[20] However, in core−shell structures, the work function of the material may be augmented as the surface coverage increases toward the intrinsic Φ of the

Received: October 5, 2016
Accepted: October 26, 2016

DOI: 10.1021/acs.jpclett.6b02293
J. Phys. Chem. Lett. 2016, 7, 4475−4482

shell material; three examples are presented schematically in Figure 1.

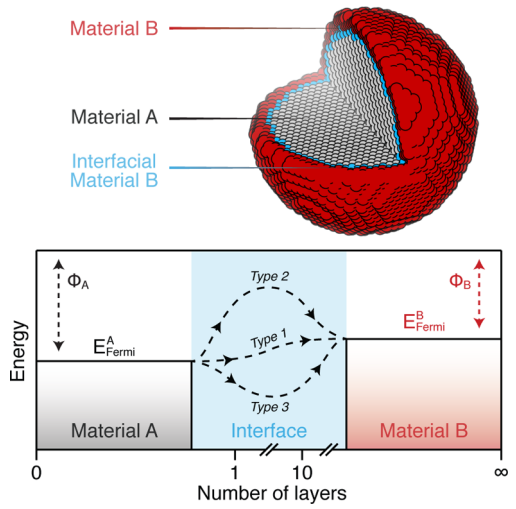

Figure 1. Electronic properties of core−shell heterostructures dependent on the composition of materials A and B. In circumstances where the isolated Fermi levels (E_{Fermi}) of materials A and B are misaligned, the work function (Φ) and other electronic properties are a function of the shell thickness. Three schematic electronic structure modulations are presented. Type 1: A smooth Fermi level transition with increasing layer thickness. Type 2: An initial Fermi level increase at low shell loading and subsequent convergence to the shell like material. Type 3: An initial Fermi level decrease at low shell loading and subsequent convergence to the shell-like material.

To further characterize the core−shell interaction, we can also examine how the absolute position of the noble metal d-band center is augmented as a function of the surface topology. Here, negative d-band center shifts are considered favorable as they correlate with decreased adsorption enthalpies of typical catalytic π-acceptor poisons, such as CO.[21−23] It should be noted that a more negative d-band centering is not desirable in all applications, particularly in instances where the reagent is required to bind strongly to the surface. The viability of Φ and the d-band center as general descriptors for catalytic reactivity are highly dependent on the surface topology descriptions.

Recovering Energetically Favorable Surface Topology. Traditionally, the monolayer (ML) noble metal surface coverage has been modeled as an idealized surface, wherein the surface atoms occupy cystallographic high symmetry points (Figure 2a).[24,25] However, the experimentally realized materials are synthesized at high temperatures, and there is no observation that suggests these symmetric points are indeed optimal. There lacks an a priori justification for a temperature-independent DFT model to recover the surface topology obtained via the high-temperature synthetic self-assembly process. Furthermore, previous reports cannot capture accurate d-band center shifts posing problems for the predictive capabilities of previous models.[26]

In this work, we use an ab initio thermal annealing computational method detailed in the Experimental Methods section to recover realistic 1 ML coverage realized through a heat, quench, and exfoliation (HQE) method. The HQE method, presented schematically in Figure 2c, can be applied to any number of supersurface coverages, and with appropriate annealing time, the HQE method should yield the thermodynamic minimum energy structure. Furthermore, this HQE method is not limited to NM-on-$Ti_{0.1}W_{0.9}C$, or explicitly to be used for the prediction of high-temperature synthetic products. DFT is intrinsically temperature-independent; even low-

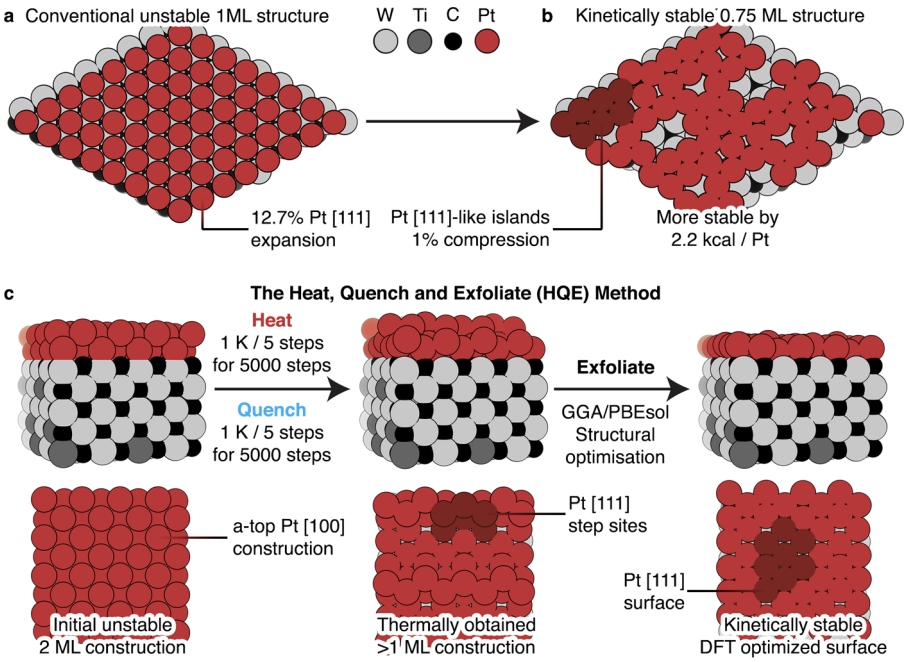

Figure 2. Conventional Pt-ML constructions (a) featuring extreme lattice mismatch between the core and surface layer. Heating and quenching the conventional structure yields a more stable sub-ML coverage. No Pt atoms were removed in panel b; the heating process causes a surface reordering that forms small [111]-like regions and pinholes exposing core TiWC. This method can be generalized to obtain realistic coverage of any surface loading through a heat, quench, and exfoliate (HQE) technique (detail in panel c). Pt has a propensity to form [111]-like coverage (emphasized in burgundy), independent of the subsurface faceting. The HQE method is performed to obtain a highly converged equilibrium structure.

DOI: 10.1021/acs.jpclett.6b02293
J. Phys. Chem. Lett. 2016, 7, 4475−4482

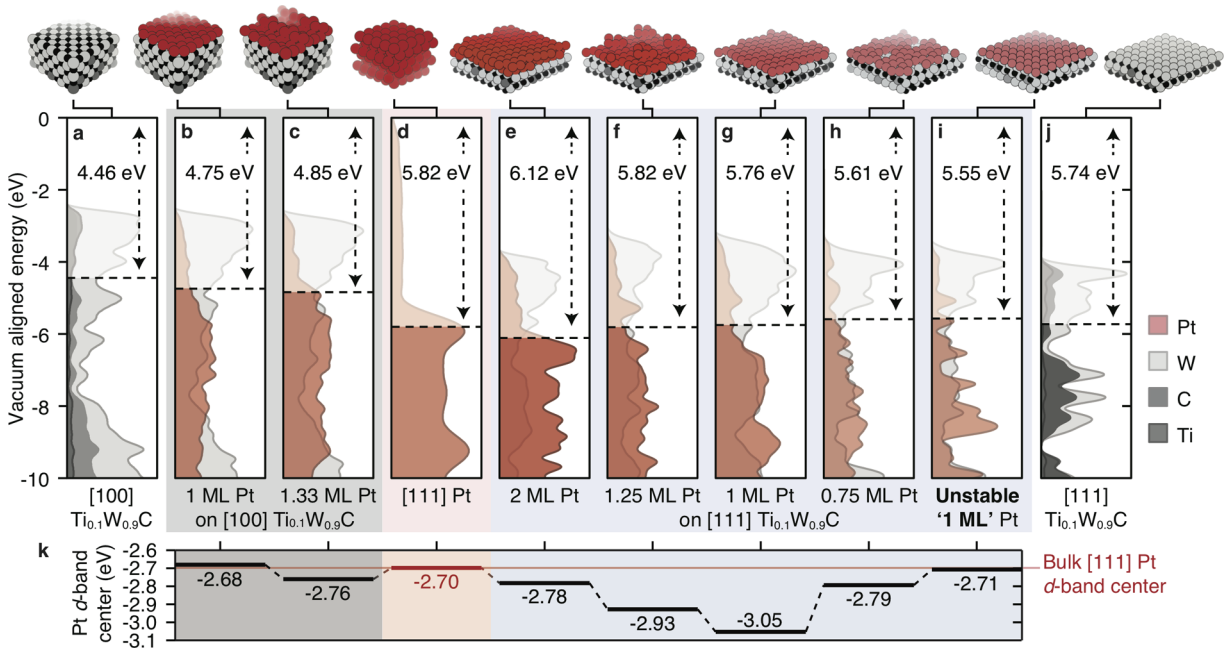

Figure 3. Surface topologies and vacuum-aligned projected density of states of [100] and [111] metal-terminated $Ti_{0.1}W_{0.9}C$ (panels a and i, respectively). Bulk [111]-Pt is included for reference (d). Using the HQE method (ab initio molecular dynamics/PBEsol), various degrees of surface coverage of Pt are obtained. The 1 ML (b) and 1.33 ML (c) Pt-coated [100]-$Ti_{0.1}W_{0.9}C$ converged to a [111]-Pt topology. Similarly, the 2, 1.25, 1, and 0.75 ML coverage of Pt on [111]-$Ti_{0.1}W_{0.9}C$ are presented in panels e–h. From the computed increased work function of 2 ML Pt on [111]-$Ti_{0.1}W_{0.9}C$ (e) relative to bulk [111]-Pt (d), we conclude that these materials are type 3 (from the schematic presented in Figure 1). The Pt d-band centers are also presented and show that the $Ti_{0.1}W_{0.9}C$ core favorably modulates their positions with exception of the minor increase shown on the 1 ML Pt on [100]-$Ti_{0.1}W_{0.9}C$ surface (k). The historical 1 ML model is included for reference (i). Ti and C density of states are excluded for clarity in panels b–i.

temperature synthesis includes infinitely more kinetic energy than conventional DFT models.

First, we sought to demonstrate that conventional reported structures with "1 ML" coverage (Figure 2a) were metastable and certainly less stable than HQE-obtained structures. In the most simple case, an idealized monolayer of Pt on [111]-$Ti_{0.1}W_{0.9}C$ is heated, quenched, and then subjected to the same DFT optimization parameters as the conventional model without the heating and cooling. The HQE method produces a structure that is substantially more stable by 2.2 kcal/Pt (Figure 2b). In this case, exfoliation was not required because we were intending to sample the sub-ML coverage. The electronic properties were also substantially altered and are discussed in detail in the following section.

To obtain a stable monolayer coverage, the HQE method requires >1 conventional ML of Pt. We elected to begin with Pt 2 MLs that were then subjected to ab initio molecular dynamics (based on DFT/GGA forces) with an applied heating gradient from 0 to 1000 K. The system is held at the maximum temperature to confirm dynamic stability. Then, the material is cooled at the same rate (quench), and the monolayer coverage (as defined by the size of the computational cell) is obtained by removal of supersurface atoms (atomistic exfoliation). Exfoliated atoms were determined by their *c*-axis coordinate: greater than 4 Å from the surface W was judiciously removed.

The heat and quench routine was performed on the true 1 ML coverage to ensure no islanding or steps were formed. Indeed, the layer remained smooth but mobile as observed by the sheet sliding across the W surface. In other words, once the ML is constructed, the mean Pt–Pt distance becomes essentially constant throughout subsequent heating.

Applying HQE to TiWC. The HQE method allows topological predictions of such surfaces to be recovered computationally via an inexpensive and efficient simulated annealing process. This procedure in principle recovers the topology of a more realistic and stable monolayer (and alternative integer and subinterger coverages) independently of the exposed core facet. In nanoparticles with fcc-$Ti_{0.1}W_{0.9}C$ cores, the surface is primarily composed of two low-index facets: [100] and W-terminated [111], shown in panels a and j of Figure 3, respectively. Using the HQE method with Pt loaded on both the [100] and W-terminated [111] surfaces of $Ti_{0.1}W_{0.9}C$, we predict that [111]-Pt coverage is unanimously preferred, independent of subsurface (core) facet (i.e., the subsurface carbide does not dictate the packing of surface-anchored Pt). The recovered coverage is very near perfect [111]-Pt; the parameters that influence this reduced mismatch are discussed in Experimental Methods and the Supporting Information.

Both $Ti_{0.1}W_{0.9}C$ surfaces coated in 1 ML of Pt converge to the [111] Pt topology. Yet, the surface electronics vary substantially for a single ML of Pt on the [100] and [111] facets of $Ti_{0.1}W_{0.9}C$ (panels b and g of Figure 3, respectively). In summary, the [100] 1 ML Pt features an average Pt–Pt distance of 2.62 Å, while the [111] has an average Pt–Pt distance is 2.70 Å. The work functions are also markedly different, with the [111] material having a Φ similar to that of bulk [111] Pt. The d-band centers are also augmented with surface dependency; the 1 ML Pt-on-[111] $Ti_{0.1}W_{0.9}C$ model exhibits a significant d-band center shift of −0.35 eV compared to bulk [111] Pt, while the Pt d-band center seems to be unperturbed in the 1 ML Pt-on-[100] $Ti_{0.1}W_{0.9}C$.

DOI: 10.1021/acs.jpclett.6b02293
J. Phys. Chem. Lett. 2016, 7, 4475–4482

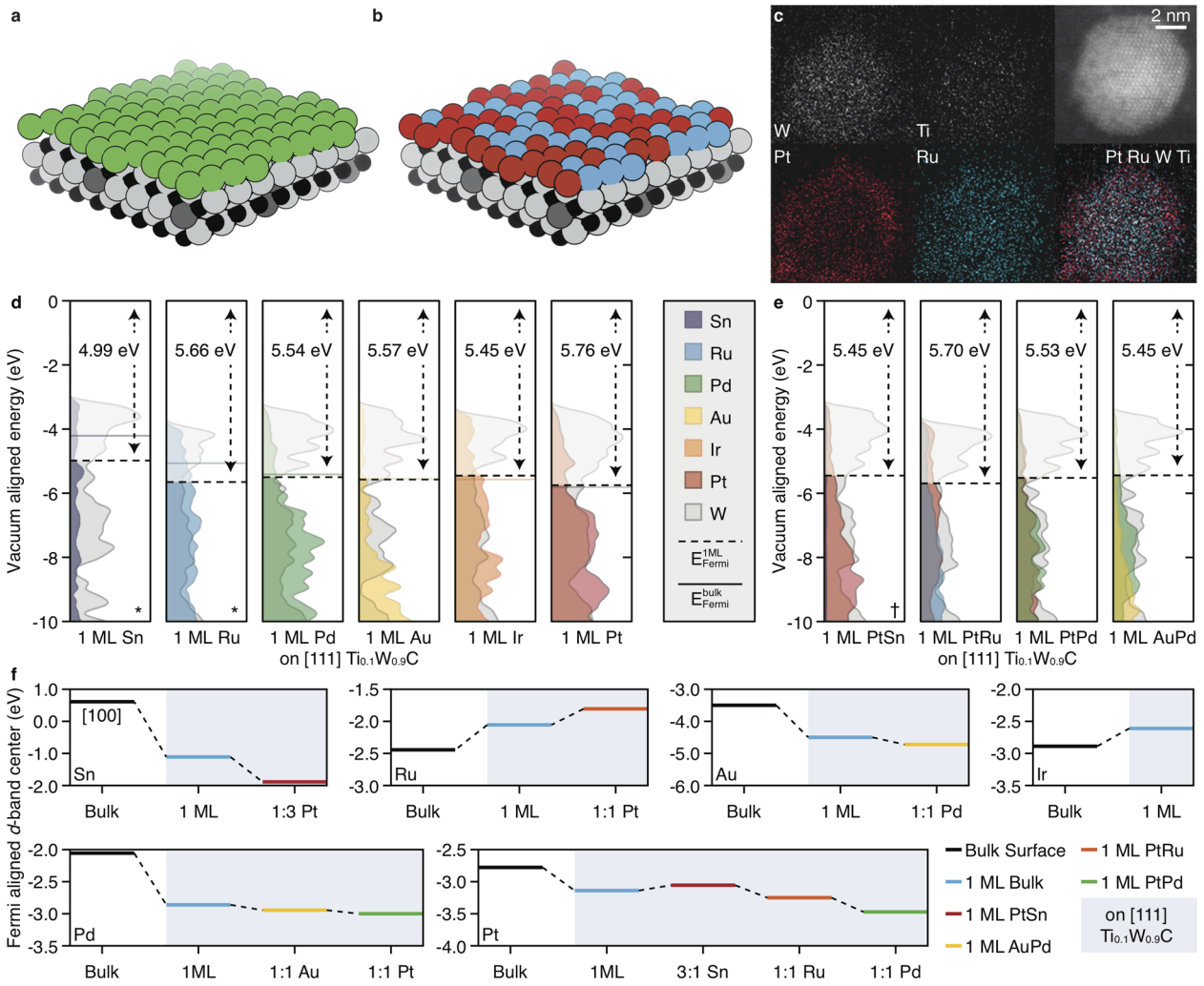

Figure 4. Representaive models for the monometallic (a) and bimetallic (b) materials. The bimetallic distribution was randomly constructed, based on the distributions observed in the EDX map of the TiWC/PtRu alloy (c). The vacuum-aligned density of states of single-element noble metal monolayer coverage on [111]-$Ti_{0.1}W_{0.9}C$ are shown in panel d. The solid-colored line overlaid on each density of states plot is the computed E_F for the bulk surface metal. Representative 1:1 alloys are presented in panel e; † indicates a 1:3 SnPt ratio. The metal d-band centers are shown in panel f. The bulk material surface is presented in black, and the elemental monolayer on [111]-$Ti_{0.1}W_{0.9}C$ in blue. Subsequent alloys and compositional ratios are labeled, and their colors correspond to their alloy. Ti and C density of states are excluded for clarity. Sn and Ru are labeled with an asterisk to indicate that reduced convergence criteria were required to optimize these materials (further details in Experimental Methods).

In summary, the HQE method predicts that there should be two types of [111]-Pt with vastly different d-band centers. Indeed, the observation of homogeneous [111]-Pt termination with differing electronic properties depending on the terminus of the core surface facet could explain the broad CO-stripping voltammograms observed in electrochemical CO-stripping voltammetry experiments.[9] In particular, the low potential peak (0.32 V vs RHE) could be attributed to the [111] 1 ML Pt-on-[111] $Ti_{0.1}W_{0.9}C$ sites, while the higher potential peak (0.74 V vs RHE) could be attributed to the [111] 1 ML Pt-on-[100] $Ti_{0.1}W_{0.9}C$ sites.[9] Such facet-dependent stripping behavior is well-known in the literature, such as for CO-stripping on Pt and Pb-stripping on Au,[27−29] and can be correlated to the differing d-band centers of the exposed facets.

Furthermore, the conventional model is also presented in Figure 3i, with its thermally annealed partner shown in Figure 3h. Here we can compare the idealized 1 ML coverage to the HQE monolayer (Figure 3g). The conventional method does not show a significant d-band shift, which would suggest that this coverage should yield no difference in CO tolerance compared to bulk Pt. This is in direct contrast to our experimental results, suggesting that the conventional method is insufficient for predicting the electronic properties of Pt on $Ti_{0.1}W_{0.9}C$.

The modulation in Pt reactivity is not limited to the subsurface facet of the core, but also the extent of monolayer coverage. Two coverages are presented for Pt loaded on [100] $Ti_{0.1}W_{0.9}C$ (Figure 3b,c), and four coverages are presented for [111] $Ti_{0.1}W_{0.9}C$ (Figure 3e−h). Given the observed work function increase to 6.12 eV for the 2 ML Pt loadings, Pt-on-$Ti_{0.1}W_{0.9}C$ is potentially a type 3 material from our models (Figure 1). Note that the d-band center reaches a synergistic minimum (−3.05 eV) at the perfect 1 ML Pt coverage. While these models do not explicitly address surface reactivity of exposed core material, the surface reactivity of submonolayer coverage will ultimately be dictated by the interplay of exposed $Ti_{0.1}W_{0.9}C$ sites and surface Pt sites. Such configurations could have interesting applications in catalytic reactions where both TMCs and NMs have high reactivity, such as reverse water−gas shift or reactions where the TMCs have comparably lower

DOI: 10.1021/acs.jpclett.6b02293
J. Phys. Chem. Lett. 2016, 7, 4475−4482

reactivity but the surface Pt decorations can serve to donate reactive intermediates to exposed TMC sites.[30]

Diversifying HQE to Other Metallic Systems. Thus far we have considered only Pt loaded on two facets of $Ti_{0.1}W_{0.9}C$ and demonstrated extensive chemical modularity as a function of surface topology. However, our recently developed experimental method lays the foundation for accessing a general array of monometallic and heterometallic noble metal monolayer alloy configurations. Besides Pt, the synthetic procedure also realized core−shell architectures with other noble metals (Au, Ru, Rh, and Ir). Here, we extend our theoretical study to other interesting elements such as Sn and Pd that should also phase-separate from carbide lattices at high temperatures. A representative 1 ML Pd on $Ti_{0.1}W_{0.9}C$ is shown in Figure 4a. The projected density of states, work functions, and their deviations from their parent bulk material are presented in Figure 4d. Both Sn and Ru required relaxed convergence criteria after the HQE procedure;[31] see the Supporting Information for further details. From work function alignments, it is clear that $Ti_{0.1}W_{0.9}C$ does not substantially modulate the surface work function for a variety of shell elements in the monometallic configuration. As such, it behaves as an ideal core material for core−shell nanoparticle design. A comparison of the bulk and 1 ML-on-$Ti_{0.1}W_{0.9}C$ d-band centers is presented in Figure 4f in black (bulk) and blue (1 ML) lines, respectively. With the exception of 1 ML Ru and Ir, all d-band centers are favorably down-shifted with respect to their bulk material surfaces. This downshift suggests that the $Ti_{0.1}W_{0.9}C$ is acting as an electron donor for Sn, Au, Pd, and Pt (making Pt and Au "more noble") but an electron sink for Ru and Ir.

Bimetallic shell alloys were constructed based on a random construction of the surface (Figure 4b), cross-referenced to a representative EDX measurement of the 2:1 PtRu material (Figure 4c). From this EDX measurement, a representative bimetallic model was constructred (Figure 4b). We elected to explore surface loadings of 1 ML PtRu alloy, the quintessential methanol electrooxidation catalyst, on $Ti_{0.1}W_{0.9}C$. For this reaction, PtRu alloys are known to be highly active at low potentials because of the enhanced water activation on Ru compared to Pt, allowing for the oxidative removal of strongly adsorbed CO species.[32] Here, the energetics are determined by the $Ti_{0.1}W_{0.9}C$ core and are predicted to result in a weakened adsorption enthalpy of CO on surface Pt (the surface energetics of Ru are not strongly modulated by the coexistence of Pt). Experimentally, it was observed that the material in Figure 4f exhibited the same bifunctional surface reactivity as bulk PtRu but with substantially enhanced rates.[9]

In addition to the classic PtRu alloy formulation, there are a variety of other bimetallic catalysts that could possibly be enhanced via this new core−shell framework. For instance, PtSn has been shown to be a highly CO-tolerant hydrogen oxidation catalyst and a highly active ethanol electrooxidation catalyst.[33,34] PtPd formulations have been shown to be highly active oxygen reduction electrocatalysts, sulfur-resistant hydrogenation catalysts, and selective reforming catalysts.[35−38] AuPd demonstrated high activity for formic acid decomposition and hydrogen peroxide direct synthesis.[39−42] The d-band centers for the bimetallics are not dramatically influenced by their coalloyed partners (Figure 4f). In all cases, the monometallic monolayer calculations (blue lines in Figure 4f) could be used as an indicator for the direction of d-band shifting in the alloyed systems. In fact, the alloys amplified the d-band shifts in all cases with exception of the PtSn alloy. Surprisingly, the 3:1 PtSn alloy reveals that the Sn contribution to the density of states is so small that it is barely visible in the density of states. The resultant material has an effective Pt loading of 0.75 ML, with a work function and d-band center similar to that of the 0.75 ML Pt-on-[111] $Ti_{0.1}W_{0.9}C$ (Figure 3h). This effect would suggest that, if these materials can be synthetically realized, Sn could be added to cover the remaining $Ti_{0.1}W_{0.9}C$ surfaces with no negative electronic effects. Furthermore, the addition of Sn is also known to have favorable water activation and antipoisoning effects for Pt catalysts, despite Sn not contributing to the surface electronics;[43] these PtSn alloys are an intriguing future synthetic avenue.

In both the monometallic and representative 1 ML AuPd alloy, the majority of Au electron density is well below E_F (in the most extreme case, the d-band center is relatively downshifted to ca. −5 eV). Indeed, Au is considered the "noblest metal";[44] there are few unoccupied states that can interact with the orbitals of adsorbed molecules, with the exception of sulfur which forms covalent bonds with surface Au sites.[45] Here we predict a further increase in the nobility of Au owing to the substantial negative d-band shift. Currently, the high activity of AuPd for H_2O_2 direct synthesis is largely attributed to Au acting as an inert spacer between the Pd ensembles. In the core−shell formulation, Au could be even more noble and the Pd more selective because of its corresponding d-band center downshift. Similarly, PtPd in a core−shell formulation could also be more selective for hydrogenations and reforming because of their favorable downshifts.

We have presented a computational procedure to more adequately describe the nature of multimetallic interfaces and their surface topology. This method was demonstrated in the context of the family of noble metal−transition-metal carbide heterostructures, which function as highly active catalysts. Application of the method has provided new insights into the origin of improved reactivity of Pt and PtRu on $Ti_{0.1}W_{0.9}C$. In addition, we have gained general predictive insights that may be used to design novel catalysts with improved chemical properties. Lastly, this general method lays the foundation for next-generation computational modeling of exotic catalysts formed via high-temperature self-assembly processes and potentially other lower-temperature syntheses in which the conventional monolayer coverage is thermodynamically less favorable than the more dense arrangement recovered by the HQE method.

EXPERIMENTAL METHODS

Standard States. All calculations were performed within the Kohn−Sham DFT framework as implemented in Vienna ab initio simulation package (VASP),[46] a planewave code (with projector augmented wave (PAW) scalar relativistic core potentials),[47] using periodic boundary conditions to approximate the infinite solids. Beginning with the crystallographic unit cells of Pt, Au, Ru, Pd, Ir, Sn, W, and WC, the lattice parameters and atomic positions were optimized using the PBEsol functional,[48] with a Γ point-centered 10 × 10 × 10 **k**-mesh and a 500 eV planewave cutoff. These criteria resulted in energies converged to at least 0.005 eV per atom. The [111] surface was then cut from each of these optimized structures (with the exception of Sn for which the [110] surface was used because it was most similar to the fcc-[111] materials). The [100]-WC surface was also constructed. The systems were then optimized to their equilibrium structures, with the cell volume

DOI: 10.1021/acs.jpclett.6b02293
J. Phys. Chem. Lett. 2016, 7, 4475−4482

fixed (to ensure the vacuum region remained intact). For these calculations, a 500 eV plane-wave cutoff basis set and a 6 × 6 × 1 **k**-mesh was found to be suitable for convergence of the systems to within 0.005 eV/atom. Because of the metallic nature of the materials, the stoichiometric [111]-WC surface did not require surface passivization.

The $Ti_{0.1}W_{0.9}C$ slab was then created by expansion to a 2 × 2 × 1 supercell with a 15 Å vacuum layer. Ti substitutions were made randomly to 10% of the W sites. The slab was then geometrically and electronically optimized with respect to atomic positions using a 2 × 2 × 1 Γ point-centered **k**-mesh and the same energetic cutoffs as the bulk materials. These parameters were found to be remarkably computationally efficient with excellent convergence (Figure S2). Convergence details, standard state density of states, and alignments are presented in the Supporting Information.

Vacuum Level Alignment. To calculate the reference electrostatic potential (vacuum level), we take an average of the Hartree potential in the vacuum region of the cell and use this as an internal reference for the electronic eigenvalues and Fermi level.[19] For example, Figure S3 shows the [110] terminated Au slab and the electrostatic potential sampling of the cell. The electrostatic potential reaches a constant in the vacuum region, and this value is then used to align the Fermi level (where $\Phi = E_F - E_{reference}$). This allows us to align Fermi levels to the vacuum and hence obtain a comparison of work function based on composition or, in the case of Figure S3, surface topology. In this case, there is very good agreement between the computed and experimentally determined values.

The analysis code for this calculation, which can also calculate planar and macroscopic averages of electrostatic potentials and charge densities, is freely available.[49] It should be noted that our alignment method works for periodic asymmetric materials if the material has metallic character. Visualizations of the structures were made using the codes VESTA.[50]

Heat, Quench, and Exfoliation Method. Without an informed initial "guess" of the surface topology, temperature-independent DFT computations of idealized surfaces struggle to recover representative descriptions of the terminal topology. The method we use here requires a construction of excessive surface layering, followed by an ab initio molecular dynamics heating process (heat) to allow for surface atoms to move into more favorable positions (Figure S1). The materials are then cooled back to their temperature-independent positions (quench), and the supersurface atoms are removed (exfoliate) to yield a representative high-temperature 1 ML coverage. The final structures are then further optimized using the GGA method used for the standard states, resulting in highly converged structures to within 0.005 eV per atom. With knowledge of the surface covering, we can construct other stoichiometric surface loadings and perform a similar process. Note that this method is general and not limited to the studies presented in this Letter.

While conventional methods of creating layers involve producing postsurface site inclusion of heavy atoms (Figure 2a), this method severely underpopulates the surface. This effect is apparent in both the lattice mismatch of the surface material (in some cases up to 15% expansion) and also the output of the computations (conventional constructions do not support the experimental CO-stripping observations).[9,51] Furthermore, if the conventional structure was indeed the global minimum, then a sufficiently slow quench should allow tempering to reproduce the starting structure. Here, this is not the case as the obtained structure in all cases was substantially more stable than their parent conventional construction.

To recover a thermodynamic minimum and true monolayer surface coverage, kinetic ab initio modeling was used to introduce heat (nuclear kinetic energy) to the slab coated in excess layers of Pt. Heating and subsequent cooling were performed by ramping "temperature" up from 0 to 1000 K in 0.1 K per 5 fs time steps in a canonical ensemble as implemented in VASP. In practice, the monolayer coverage is obtained at around "50 K" in the heating process. Subsequent heating was used to assess dynamic stability and core−shell mixing; in all cases, the core structure was maintained (no surface W reordering was observed). The maximum temperature was maintained for 50 time steps, and then the system was cooled again at the same rate. Relaxed convergence criteria (0.1 eV/atom), a reduced planewave basis (400 eV cutoff), and a reduced **k**-grid (Γ-point only) are required for the heating and cooling processes, but the terminal geometries are treated with the typical DFT optimization parameters as stipulated above, and the energetics are compared from the DFT-optimized HQE structures.

All atoms were allowed to move throughout the heating and cooling processes to assess dynamic stability. An animation of one representative event (the heating of 1.3 conventional ML) is provided in the Supporting Information. The HQE method yields a more realistic Pt−Pt spacing (comparable to bulk [111] terminated Pt) (Table S1), is highly converged, and rationalizes several enigmatic experimental findings. Note that the HQE method does not yield a single unique structure for the noninteger coverage, but the variations in the structure seemed to have negligible impact on the electronic properties. In summary, the HQE method produces valuable surface configurations which are otherwise unattainable by conventional DFT methods. This method was used for all coverages presented in this Letter.

For comparison, the DFT-optimized Pt−Pt distance of bulk [111]-Pt gives a lateral bond length of 2.76 Å (Figure 2a). However, the "idealized surface" (high symmetry points) of Pt on [111]-$Ti_{0.1}W_{0.9}C$ typically invoked in the literature features a Pt−Pt distance of 3.00 Å. On [0001]-W_2C, the Pt−Pt distance is even larger (3.11 Å). This requires a lattice mismatch of 8.7% and 12.7%, respectively. Such an expanded bond length is on the verge of being epitaxially unfavorable,[52] and this strain installs significant electronic property differences[51,53,54] compared to those described here. The HQE method yields a more reasonable average Pt−Pt distance of 2.70 Å on [111]-$Ti_{0.1}W_{0.9}C$. This structure features an increase in surface Pt loading of 33% compared to the conventional method and is in agreement with experimental results showing that Pt monolayers self-assemble onto the surface of WC at elevated temperatures above the Tammann point for Pt.[9]

Aberration-Corrected STEM with EDX Mapping and Linescans. Aberration-corrected scanning transmission electron microscopy (STEM) with energy-dispersive X-ray (EDX) mapping and linescans (Figure 4c) was performed on an FEI equipped with a CEOS probe-side aberration corrector operated at 200 kV, with a probe convergence angle of 24.5 mrad, to validate the dispersion of metals in the bimetallic systems. High-angle annular dark-field (HAADF) mode was used for imaging, with a probe current of ca. 25 pA and spatial resolution <0.1 nm. Energy-dispersive spectrometry (EDS) images were taken (EDAX EDS detector, 128 eV resol.) with a probe current

DOI: 10.1021/acs.jpclett.6b02293
J. Phys. Chem. Lett. 2016, 7, 4475−4482

ca. 200−780 pA and spatial resolution ca. 0.16−0.29 nm. Sample preparation for STEM included dispersion in acetone, ultrasonication for 30 min, and then deposition onto carbon copper TEM grids. STEM samples were plasma cleaned for 15 min before being loaded into the microscope.

■ ASSOCIATED CONTENT

Supporting Information

The Supporting Information is available free of charge on the ACS Publications website at DOI: 10.1021/acs.jpclett.6b02293.

Convergence details, electrostatic alignment procedure, and structural details (PDF)

Animated Heating and Quenching (GIF)

■ AUTHOR INFORMATION

Corresponding Authors

*E-mail: hendon@mit.edu.

*E-mail: yroman@mit.edu.

Notes

The authors declare no competing financial interest.

■ ACKNOWLEDGMENTS

Work at MIT was supported by the Department of Energy, Office of Basic Energy Sciences (DE-SC0016214). S.T.H. thanks the National Science Foundation (Graduate Research Fellowship Grant 1122374), and M.M. thanks the Swiss National Science Foundation (Project P2EZP2_159124) for financial support. A.W. is supported by the Royal Society and the ERC (Grant 277757). The computational work was facilitated by access to the UK National Supercomputer, ARCHER (EPSRC Grant EP/L000202) and access to the Extreme Science and Engineering Discovery Environment (XSEDE), which is supported by National Science Foundation Grant ACI-1053575.[55] We are grateful for the EDX measurements performed by J. A. Dumesic and A. C. Alba-Rubio.

■ REFERENCES

(1) Strasser, P.; et al. Lattice-strain control of the activity in dealloyed core-shell fuel cell catalysts. *Nat. Chem.* **2010**, *2*, 454−60.

(2) Yang, H. Platinum-Based Electrocatalysts with Core-Shell Nanostructures. *Angew. Chem., Int. Ed.* **2011**, *50*, 2674−2676.

(3) Guo, S.; Zhang, S.; Sun, S. Tuning Nanoparticle Catalysis for the Oxygen Reduction Reaction. *Angew. Chem., Int. Ed.* **2013**, *52*, 8526−8544.

(4) Bell, A. T. The Impact of Nanoscience on Heterogeneous Catalysis. *Science* **2003**, *299*, 1688−1691.

(5) Kitchin, J.; Nørskov, J. K.; Barteau, M.; Chen, J. Modification of the surface electronic and chemical properties of Pt (111) by subsurface 3d transition metals. *J. Chem. Phys.* **2004**, *120*, 10240−10246.

(6) Nørskov, J. K.; Bligaard, T.; Logadottir, A.; Kitchin, J. R.; Chen, J. G.; Pandelov, S.; Stimming, U. Trends in the Exchange Current for Hydrogen Evolution. *J. Electrochem. Soc.* **2005**, *152*, J23.

(7) Hunt, S. T.; Nimmanwudipong, T.; Roman-Leshkov, Y. Engineering non-sintered, metal-terminated tungsten carbide nanoparticles for catalysis. *Angew. Chem., Int. Ed.* **2014**, *53*, 5131−5136.

(8) Hunt, S. T.; Kokumai, T. M.; Zanchet, D.; Román-Leshkov, Y. Alloying Tungsten Carbide Nanoparticles with Tantalum: Impact on Electrochemical Oxidation Resistance and Hydrogen Evolution Activity. *J. Phys. Chem. C* **2015**, *119*, 13691−13699.

(9) Hunt, S. T.; Milina, M.; Alba-Rubio, A. C.; Hendon, C. H.; Dumesic, J. A.; Román-Leshkov, Y. Self-assembly of noble metal monolayers on transition metal carbide nanoparticle catalysts. *Science* **2016**, *352*, 974−978.

(10) Hunt, S. T.; Milina, M.; Wang, Z.; Román-Leshkov, Y. Activating earth-abundant electrocatalysts for efficient, low-cost hydrogen evolution/oxidation: sub-monolayer platinum coatings on titanium tungsten carbide nanoparticles. *Energy Environ. Sci.* **2016**, *9*, 3290−3301.

(11) Kitchin, J. R.; Nørskov, J. K.; Barteau, M. A.; Chen, J. G. Trends in the chemical properties of early transition metal carbide surfaces: A density functional study. *Catal. Today* **2005**, *105*, 66−73.

(12) Stephens, I. E.; Bondarenko, A. S.; Grønbjerg, U.; Rossmeisl, J.; Chorkendorff, I. Understanding the electrocatalysis of oxygen reduction on platinum and its alloys. *Energy Environ. Sci.* **2012**, *5*, 6744−6762.

(13) Schaidle, J. A.; Schweitzer, N. M.; Ajenifujah, O. T.; Thompson, L. T. On the preparation of molybdenum carbide-supported metal catalysts. *J. Catal.* **2012**, *289*, 210−217.

(14) Michalsky, R.; Zhang, Y. J.; Medford, A. J.; Peterson, A. A. Departures from the adsorption energy scaling relations for metal carbide catalysts. *J. Phys. Chem. C* **2014**, *118*, 13026−13034.

(15) Esposito, D. V.; Chen, J. G. Monolayer platinum supported on tungsten carbides as low-cost electrocatalysts: opportunities and limitations. *Energy Environ. Sci.* **2011**, *4*, 3900−3912.

(16) Lang, N.; Kohn, W. Theory of metal surfaces: work function. *Phys. Rev. B* **1971**, *3*, 1215.

(17) Michaelson, H. B. The work function of the elements and its periodicity. *J. Appl. Phys.* **1977**, *48*, 4729−4733.

(18) Scanlon, D. O.; et al. Band alignment of rutile and anatase TiO2. *Nat. Mater.* **2013**, *12*, 798−801.

(19) Butler, K. T.; Hendon, C. H.; Walsh, A. Electronic chemical potentials of porous metal-organic frameworks. *J. Am. Chem. Soc.* **2014**, *136*, 2703.

(20) Vayenas, C. G.; Bebelis, S.; Ladas, S. Dependence of catalytic rates on catalyst work function. *Nature* **1990**, *343*, 625−627.

(21) Hammer, B.; Morikawa, Y.; Nørskov, J. K. CO chemisorption at metal surfaces and overlayers. *Phys. Rev. Lett.* **1996**, *76*, 2141.

(22) Ruban, A.; Hammer, B.; Stoltze, P.; Skriver, H. L.; Nørskov, J. K. Surface electronic structure and reactivity of transition and noble metals. *J. Mol. Catal. A: Chem.* **1997**, *115*, 421−429.

(23) Leonard, K. C.; Bard, A. J. Pattern Recognition Correlating Materials Properties of the Elements to Their Kinetics for the Hydrogen Evolution Reaction. *J. Am. Chem. Soc.* **2013**, *135*, 15885−15889.

(24) Esposito, D. V.; Hunt, S. T.; Stottlemyer, A. L.; Dobson, K. D.; McCandless, B. E.; Birkmire, R. W.; Chen, J. G. Low-cost hydrogen-evolution catalysts based on monolayer platinum on tungsten monocarbide substrates. *Angew. Chem., Int. Ed.* **2010**, *49*, 9859−9862.

(25) Esposito, D. V.; Hunt, S.; Kimmel, Y. C.; Chen, J. G. A new class of electrocatalysts for hydrogen production from water electrolysis: metal monolayers supported on low-cost transition metal carbides. *J. Am. Chem. Soc.* **2012**, *134*, 3025−3033.

(26) Yu, W.; Porosoff, M. D.; Chen, J. G. Review of Pt-Based Bimetallic Catalysis: From Model Surfaces to Supported Catalysts. *Chem. Rev.* **2012**, *112*, 5780−5817.

(27) Finot, M. O.; Braybrook, G. D.; McDermott, M. T. Characterization of electrochemically deposited gold nanocrystals on glassy carbon electrodes. *J. Electroanal. Chem.* **1999**, *466*, 234−241.

(28) Maillard, F.; Eikerling, M.; Cherstiouk, O.; Schreier, S.; Savinova, E.; Stimming, U. Size effects on reactivity of Pt nanoparticles in CO monolayer oxidation: The role of surface mobility. *Faraday Discuss.* **2004**, *125*, 357−377.

(29) Zhdanov, V. P.; Kasemo, B. Simulation of CO electrooxidation on nm-sized supported Pt particles: stripping voltammetry. *Chem. Phys. Lett.* **2003**, *376*, 220−225.

(30) Porosoff, M. D.; Yang, X.; Boscoboinik, J. A.; Chen, J. G. Molybdenum Carbide as Alternative Catalysts to Precious Metals for Highly Selective Reduction of CO2 to CO. *Angew. Chem., Int. Ed.* **2014**, *53*, 6705−6709.

(31) Jackson, A. J.; Skelton, J. M.; Hendon, C. H.; Butler, K. T.; Walsh, A. Crystal structure optimization using an auxiliary equation of

DOI: 10.1021/acs.jpclett.6b02293
J. Phys. Chem. Lett. 2016, 7, 4475−4482

state Crystal structure optimization using an auxiliary equation of state. *J. Chem. Phys.* **2015**, *143*, 184101.
(32) Schmidt, T. J.; Gasteiger, H. A.; Behm, R. J. Methanol electrooxidation on a colloidal PtRu-alloy fuel-cell catalyst. *Electrochem. Commun.* **1999**, *1*, 1−4.
(33) Liu, Z.; Jackson, G. S.; Eichhorn, B. W. PtSn intermetallic, core-shell, and alloy nanoparticles as CO-tolerant electrocatalysts for H2 oxidation. *Angew. Chem., Int. Ed.* **2010**, *49*, 3173−6.
(34) Vigier, F.; Coutanceau, C.; Hahn, F.; Belgsir, E.; Lamy, C. On the mechanism of ethanol electro-oxidation on Pt and PtSn catalysts: electrochemical and in situ IR reflectance spectroscopy studies. *J. Electroanal. Chem.* **2004**, *563*, 81−89.
(35) Chen, Z.; Waje, M.; Li, W.; Yan, Y. Supportless Pt and PtPd Nanotubes as Electrocatalysts for Oxygen-Reduction Reactions. *Angew. Chem., Int. Ed.* **2007**, *46*, 4060−4063.
(36) Navarro, R.; Pawelec, B.; Trejo, J.; Mariscal, R.; Fierro, J. Hydrogenation of aromatics on sulfur-resistant PtPd bimetallic catalysts. *J. Catal.* **2000**, *189*, 184−194.
(37) Blomsma, E.; Martens, J.; Jacobs, P. Isomerization and hydrocracking of heptane over bimetallic bifunctional PtPd/H-beta and PtPd/USY zeolite catalysts. *J. Catal.* **1997**, *165*, 241−248.
(38) Wang, X.; et al. Palladium-platinum core-shell icosahedra with substantially enhanced activity and durability towards oxygen reduction. *Nat. Commun.* **2015**, *6*, 7594.
(39) Huang, Y.; Zhou, X.; Yin, M.; Liu, C.; Xing, W. Novel PdAu@Au/C core-shell catalyst: Superior activity and selectivity in formic acid decomposition for hydrogen generation. *Chem. Mater.* **2010**, *22*, 5122−5128.
(40) Ham, H. C.; Hwang, G. S.; Han, J.; Nam, S. W.; Lim, T. H. On the Role of Pd Ensembles in Selective H2O2 Formation on PdAu Alloys. *J. Phys. Chem. C* **2009**, *113*, 12943−12945.
(41) Edwards, J. K.; Solsona, B.; Ntainjua, E.; Carley, A. F.; Herzing, A. A.; Kiely, C. J.; Hutchings, G. J. Switching off hydrogen peroxide hydrogenation in the direct synthesis process. *Science* **2009**, *323*, 1037−1041.
(42) Alba-Rubio, A. C.; Plauck, A.; Stangland, E. E.; Mavrikakis, M.; Dumesic, J. A. Direct Synthesis of Hydrogen Peroxide Over Au-Pd Catalysts Prepared by Electroless Deposition. *Catal. Lett.* **2015**, *145*, 2057−2065.
(43) Pinto, L. M.; Maia, G. Selected properties of Pt(111) modified surfaces: A DFT study. *Electrochem. Commun.* **2015**, *60*, 135−138.
(44) Hammer, B.; Nørskov, J. Why gold is the noblest of all the metals. *Nature* **1995**, *376*, 238−240.
(45) Grönbeck, H.; Curioni, A.; Andreoni, W. Thiols and Disulfides on the Au(111) Surface: The Headgroup-Gold Interaction. *J. Am. Chem. Soc.* **2000**, *122*, 3839−3842.
(46) Kresse, G.; Furthmüller, J. Efficient iterative schemes for ab initio total-energy calculations using a plane-wave basis set. *Phys. Rev. B: Condens. Matter Mater. Phys.* **1996**, *54*, 11169.
(47) Blöchl, P. Projector augmented-wave method. *Phys. Rev. B: Condens. Matter Mater. Phys.* **1994**, *50*, 17953.
(48) Perdew, J. P.; Ruzsinszky, A.; Csonka, G. I.; Vydrov, O. A.; Scuseria, G. E.; Constantin, L. A.; Zhou, X.; Burke, K. Restoring the Density-Gradient Expansion for Exchange in Solids and Surfaces. *Phys. Rev. Lett.* **2008**, *100*, 136406.
(49) Butler, K. T. MacroDensity. https://github.com/WMD-Bath/MacroDensity (accessed October 25, 2016).
(50) Momma, K.; Izumi, F. *VESTA3* for three-dimensional visualization of crystal, volumetric and morphology data. *J. Appl. Crystallogr.* **2011**, *44*, 1272.
(51) Kitchin, J. R.; Nørskov, J. K.; Barteau, M. A.; Chen, J. G. Role of Strain and Ligand Effects in the Modification of the Electronic and Chemical Properties of Bimetallic Surfaces. *Phys. Rev. Lett.* **2004**, *93*, 156801.
(52) Chang, T.-M.; Carter, E. A. Mean-field theory of heteroepitaxial thin metal film morphologies. *Surf. Sci.* **1994**, *318*, 187.
(53) Mavrikakis, M.; Hammer, B.; Nørskov, J. K. Effect of strain on the reactivity of metal surfaces. *Phys. Rev. Lett.* **1998**, *81*, 2819.
(54) Zhuang, H.; Tkalych, A. J.; Carter, E. A. Understanding and Tuning the Hydrogen Evolution Reaction on Pt-Covered Tungsten Carbide Cathodes. *J. Electrochem. Soc.* **2016**, *163*, F629−F636.
(55) Towns, J.; Cockerill, T.; Dahan, M.; Foster, I.; Gaither, K.; Grimshaw, A.; Hazlewood, V.; Lathrop, S.; Lifka, D.; Peterson, G. D.; et al. XSEDE: Accelerating Scientific Discovery. *Comput. Sci. Eng.* **2014**, *16*, 62−74.

DOI: 10.1021/acs.jpclett.6b02293
J. Phys. Chem. Lett. 2016, 7, 4475−4482